Article

A Methodological Approach for Interpreting and Comparing the Viscoelastic Behaviors of Soft Biological Tissues and Hydrogels at the Cell-Length Scale

Marta Tosini [1,2,3], Torne Tänzer [4], Simona Villata [2,5], Désirée Baruffaldi [2,5], Valentina Monica [6,7], Barbara Peracino [8], Luca Primo [6,7], Francesca Frascella [2,3,5], Fabrizio Pirri [2,5], Alberto Audenino [1,2], Diana Massai [1,2,3] and Gianpaolo Serino [1,2,3,*]

1   Department of Mechanical and Aerospace Engineering (DIMEAS), Politecnico di Torino, 10129 Turin, Italy; marta.tosini@polito.it (M.T.); alberto.audenino@polito.it (A.A.); diana.massai@polito.it (D.M.)
2   PolitoBIOMedLab, Politecnico di Torino, 10129 Turin, Italy; simona.villata@polito.it (S.V.); desiree.baruffaldi@polito.it (D.B.); francesca.frascella@polito.it (F.F.); fabrizio.pirri@polito.it (F.P.)
3   Centro 3R: Interuniversity Center for the Promotion of the 3Rs Principles in Teaching and Research, Università di Pisa, 56122 Pisa, Italy
4   Mechanical Engineering, École Polytechnique Fédérale de Lausanne, 1015 Lausanne, Switzerland; torne.tanzer@epfl.ch
5   Department of Applied Sciences (DISAT), Politecnico di Torino, 10129 Turin, Italy
6   Department of Oncology, University of Torino, 10043 Orbassano, Italy; valentina.monica@unito.it (V.M.); luca.primo@unito.it (L.P.)
7   Candiolo Cancer Institute, FPO-IRCCS, 10060 Candiolo, Italy
8   Department of Clinical and Biological Sciences, University of Torino, 10043 Orbassano, Italy; barbara.peracino@unito.it
*   Correspondence: gianpaolo.serino@polito.it

Abstract: The behavior of a cell is strongly influenced by the physical properties and stimuli in its microenvironment. Furthermore, the activation and modulation of mechanotransduction pathways are involved in tissue development and homeostasis and even pathological processes. Thus, when developing materials aimed at mimicking the extracellular matrixes of healthy or pathological tissues, their mechanical features should be closely considered. In this context, nanoindentation represents a powerful technique for mechanically characterizing biological tissues and hydrogels at the cell-length scale. However, standardized experimental protocols and data analysis techniques are lacking. Here, we proposed a methodological approach based on the nanoindentation technique for quantitatively analyzing and comparing the time-dependent load relaxation responses of soft biological tissues and hydrogels. As this was an explanatory study, stress-relaxation nanoindentation tests were performed on samples of pig and human lung tissues and of a specific gelatin-methacryloyl (GelMA) hydrogel to quantify and compare their viscoelastic properties. The proposed method allowed for identifying the characteristic parameters needed for describing the behavior of each sample, permitting us to quantitatively compare their mechanical behaviors. All samples showed load relaxation at a defined indentation depth because of their intrinsic viscoelastic behaviors, and the GelMA samples showed the highest relaxation capabilities. The distribution of the characterization parameters showed that the biological samples presented similar time-dependent responses, while differences were observed in the GelMA samples. Overall, the proposed methodological approach allows for providing key insights into the time-dependent behaviors of soft biological tissues and hydrogels at the cell-length scale in view of supporting tissue engineering and pathophysiological investigations.

Keywords: nanoindentation; viscoelastic characterization; soft tissue biomechanics; constitutive model; mechanotransduction

1. Introduction

The ability of a cell to sense and respond to mechanical cues from its microenvironment is a fundamental process known as mechanotransduction. This intricate phenomenon plays a crucial role in a wide range of cellular functions, including cell adhesion, migration, differentiation, tissue development, and homeostasis [1]. Cellular mechanotransduction is further involved in several pathophysiological processes and is being considered for its potential as a therapeutic target [2].

In the last two decades, researchers have focused on how the mechanical properties of biological tissues and their extracellular matrixes (ECMs) influence a cell's response, investigating mostly their elastic properties [3–10]. However, soft biological tissues exhibit a time-dependent mechanical behavior characterized by significant stress relaxation in response to a prescribed deformation [11], and the viscous properties of these tissues have emerged recently as key elements that influence cellular behavior [12–15]. Soft biological tissues show a viscoelastic nature that arises from the combined effects of their elastic and viscous properties, characterizing their instantaneous and time-dependent responses, respectively. The global mechanical response of soft biological tissues is due to micro-scale reactions and rearrangements of a cell's cytoskeleton and ECM biopolymers, and it is influenced by their unique molecular compositions, microstructures, and hydration levels. Thus, in view of investigating the activated signaling pathways and related cellular responses involved in mechanotransduction processes, it is crucial to characterize the viscoelastic behaviors of soft biological tissues at the cell-length scale and fabricate materials mimicking their mechanical features.

In this context, several materials and substrates have been developed, and it has been demonstrated that by tailoring their characteristics (e.g., stiffness, surface, chemistry, and topography), it is possible to influence cultured cells and direct their development in a desirable way [16–18]. For example, polyacrylamide (PAM) gels and polydimethylsiloxane (PDMS) substrates, functionalized with ECM proteins, have been widely adopted in mechanotransduction studies because of their well-defined manufacturing protocols, which guarantee the robust and reproducible control of the substrate's stiffness [14,19,20]. Hydrogels, composed of cross-linked polymer networks that can absorb and retain water [12,21–23], have emerged as promising materials for replicating a cell's microenvironment for mechanotransduction studies and tissue engineering applications [24,25]. However, their viscoelastic properties have not been fully investigated [13,14], and in order to mimic the native viscoelasticity, new design guidelines for the next-generation manufacture of hydrogels are needed.

Therefore, it has become crucial to develop a robust methodological approach for characterizing the viscoelastic properties of soft biological tissues and hydrogels. In clinical scenarios, several approaches have been developed for assessing the stiffness and viscoelasticity of biological tissues in a non-invasive way, including ultrasound elastography [26–29], magnetic resonance elastography (MRE) [30,31], and optical coherence elastography (OCE) [32–34]. On the other hand, in experimental lab settings, techniques such as tensile and compression testing [35,36], dynamic mechanical analysis (DMA), and nanoindentation [11,37–40] have been adopted to quantitatively characterize the viscoelastic behaviors of biological soft tissues and hydrogels. In particular, nanoindentation has emerged as a powerful tool as it offers the advantage of characterizing mechanical properties at the cell-length scale with high precision and spatial resolution. Furthermore, nanoindentation allows for a localized property assessment, which is particularly relevant given the hierarchical and heterogenous natures of biological tissues [41,42]. Although the viscoelastic properties of different soft tissues (e.g., murine heart [11], kidney [11], liver [11,43] cornea [44], periodontal ligament [45], cartilage [42], and brain tissues [43,46]) and of a variety of hydrogels [47–49] have been investigated through different techniques, the standardization of the applied testing protocols and data analysis methods remain a challenge. The development of standardized approaches to evaluate their viscoelastic

behaviors at the micro-scale would ensure the reproducibility and reliability of the results, enabling meaningful comparisons across different studies and laboratories.

Driven by this need, we developed a robust methodological approach for testing and analyzing the viscoelastic properties of soft biological tissues and hydrogels at the cell-scale length. In detail, the nanoindentation technique was adopted for characterizing the viscoelastic properties of samples of pig and human lung tissues and of a specific gelatin-methacryloyl (GelMA) hydrogel that was designed for replicating the native mechanical properties of human lung tissue. The tests were performed, and we controlled the indentation depth of the nanoindenter's tip into the sample's surface. To extract the parameters that characterized the sample's viscoelasticity, the generated experimental curves were analyzed through a novel approach based on the use of a genetic algorithm [45]. In addition, time parameters were not assigned as predefined values, but rather, an interval of possible values was defined to restrict the number of feasible solutions for the algorithm. Thus, instead of the commonly adopted least-square optimization algorithm, a more robust approach, based on the genetic algorithm, was developed, reducing the probability of incurring local minima and improving the fitting procedure [50–52].

2. Materials and Methods

2.1. Sample Preparation

To assess the reliability of the methodological approach proposed for characterizing the viscoelastic properties of soft biological tissues and hydrogels, samples of pig and human lung tissues and a specific GelMA hydrogel were tested.

The samples of pig lung tissue were obtained from a local butcher, cut ($2 \times 1 \times 1$ cm^3), and glued on the bottom of a plastic Petri dish. The samples were subsequently covered with phosphate buffered saline (PBS, tablets by Medicago, Uppsala, Sweden) and maintained at 37 °C until the test was performed to avoid dehydration. In total, 2 samples were tested on their cross-sectional surfaces, as reported in Figure 1a.
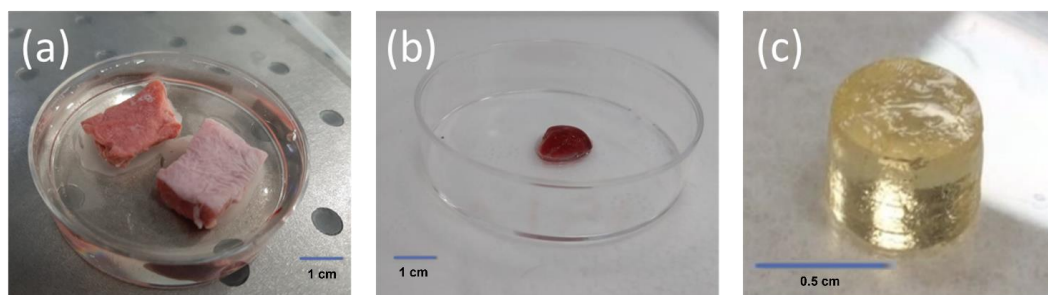
Figure 1. The tested samples: (**a**) pig lung sample (cross-section on the left and whole sample on the right); (**b**) human lung sample; and (**c**) GelMA sample.

A human lung tissue sample was obtained from a donor patient treated by lobectomy at the Candiolo Cancer Institute (Candiolo, Torino, Italy). The sample size was $1 \times 0.5 \times 0.5$ cm^3. The donor patient provided informed consent. The study was conducted under the approval of the Review Boards of the Institutions (PROFILING protocol no. 001-IRCC-00IIS-10). The clinical data were entered and maintained in the protocol owner' prospective database. The deidentified information in this study was published in accordance with the ethics guidelines of the PROFILING protocol.

The human lung sample was directly glued to a Petri dish and covered with the cell culture medium RPMI 1640, which was supplemented with 10 v/v% of fetal bovine serum (Sigma-Aldrich), and it was maintained at 37 °C (Figure 1b).

The GelMA samples were synthesized following a previously developed protocol [53]. Briefly, gelatin from bovine skin (10 g) was added to 100 mL of warm Dulbecco's phosphate buffer saline (DPBS) and stirred in rotating conditions on a heating plate at 50 °C to obtain a uniform gelatin solution. Next, 8 mL of methacrylic anhydride (MA) were slowly

added to the gelatin to obtain the desired methacrylation degree, and the reaction lasted for 2 h at 50 °C under continuous stirring. Then, the solution was diluted in 100 mL of preheated DPBS to stop the reaction, obtaining a final volume of 200 mL which was, then dialyzed against distilled water with cellulose membrane (D9527 by Sigma-Aldrich, St. Louis, MO, USA) with a molecular weight cutoff of 12–14 kDa at 40 °C for 7 days to remove all unreacted species. Lastly, the dialyzed solutions were stored at −80 °C for a minimum of 48 h before being lyophilized and stored at room temperature in the dark until further use. Before the nanoindentation tests, the GelMA samples were prepared by photo-polymerization. At first, the freeze-dried GelMA was dissolved at 10 $w/v\%$ at 37 °C in RPMI supplemented with 2.5 mg/mL of the photo initiator, lithium phenyl-2,4,6-trimethylbenzoylphosphinate (LAP by Sigma-Aldrich, St. Louis, MO, USA), and then it was left in the dark until complete dissolution at 37 °C. For each sample, 0.05 mL of solution were transferred to a dedicated mold. Afterwards, the samples were exposed to a fibre lamp (wavelength of 405 nm, dose of 3.3 mW/cm^2) for 5 min, allowing the photo-crosslinking to occur. The GelMA samples were stored in an incubator at 37 °C and analyzed the next day.

2.2. Experimental Procedure

The nanoindentation tests were performed using a Piuma nanoindenter (Optics11 Life, Amsterdam, The Netherlands) (Figure 2a). Briefly, the indenter head was mounted on a probe, comprising a reflective cantilever and a spherical tip. Samples with different mechanical properties could be tested by selecting the most suitable combination of cantilever stiffness (k_c) and tip radius (R). For this study, a probe with $k_c = 0.025$ N/m and $R = 25.5$ μm was selected.
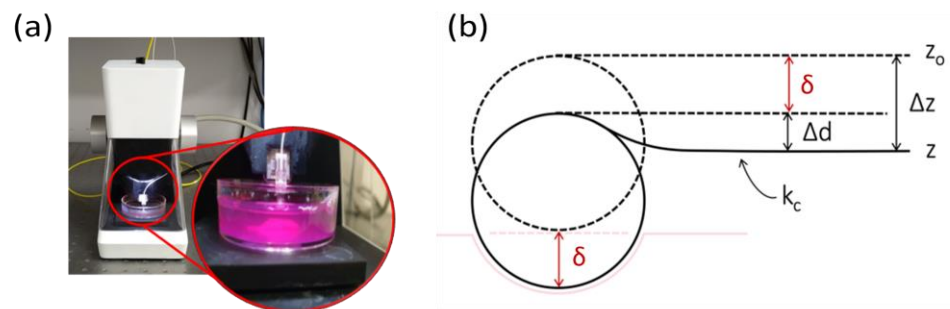
Figure 2. (**a**) Piuma nanoindenter (Optics11 Life). (**b**) Schematic representation of the cantilever/probe–sample contact, where k_c is the cantilever stiffness, δ is the indentation depth, and Δz and Δd are the total displacements covered by the probe and the cantilever bending, respectively.

A standard nanoindentation test consists of 3 distinct phases: (*i*) the loading phase, which begins when the probe touches the surface of the sample and the cantilever starts to bend (Figure 2b); (*ii*) the holding phase, which starts when a set load (P) or indentation depth (δ) is reached and kept constant for a defined time period; and (*iii*) the unloading phase, during which the probe is retracted from the surface of the sample.

Figure 3a shows a typical nanoindentation input curve, where the set indentation depth needs to be reached and held constant for a specific holding period ($t = 5$ s). Ideally, the set indentation depth should be reached through an impulsive load ($\delta(t = 0) \equiv \delta_{max}$; $P(t = 0) \equiv P_{max}$), but due to practical limitations, the maximum load (P_{max}) required to reach the set indentation depth (δ_{max}) is often applied within a finite ramp time. Figure 3b shows an explanatory load vs time curve in which the load relaxation portion (from P_0 to P_∞) is isolated in order to be analyzed and to evaluate the viscoelastic parameters. Figure 3c shows the corresponding indentation depth vs load curve.
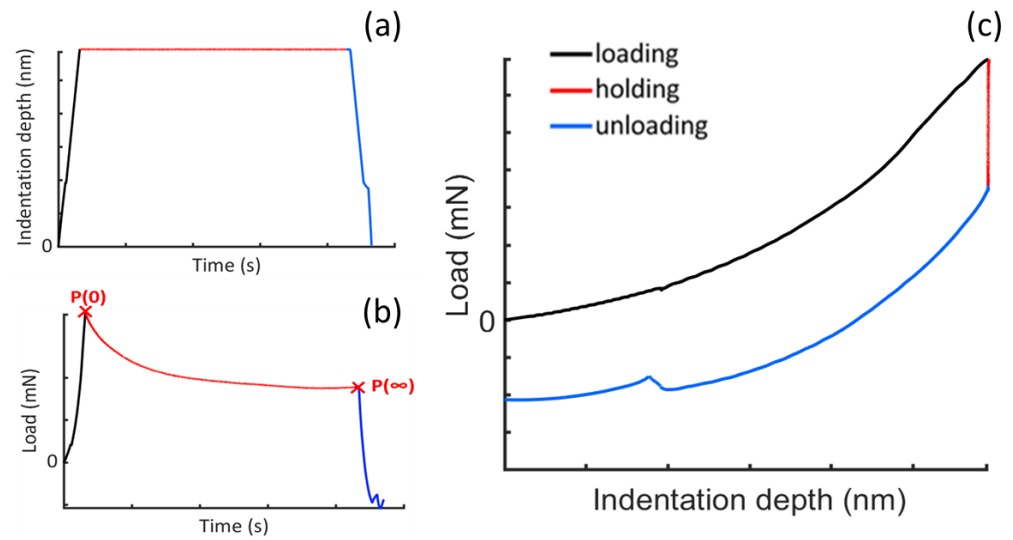
Figure 3. Nanoindentation curves during an explanatory stress–relaxation test: (**a**) indentation depth vs. time (δ-t) curve; (**b**) load vs time (P-t) curve; and (**c**) indentation depth vs load (δ-P) curve.

The applied load and the indentation depth were derived as follows:

$$\delta = (z - z_0) - (d - d_0) = \Delta z - \Delta d \text{ and} \tag{1}$$

$$P = k_c \cdot \Delta d, \tag{2}$$

where z and d are the displacements along the vertical z-axis of the probe and of the cantilever bending, respectively; z_0 and d_0 are the respective values at the contact point; and Δz and Δd are the total displacements covered by the probe and the cantilever bending, respectively. The end of the loading phase of the δ-P curve (Figure 3c) was used to derive the shear modulus corresponding to the onset of the relaxation period [54–56].

All tests were performed in hydrated conditions (in PBS for the pig lung and GelMA samples and in a cell-culture medium for human lung sample) at a temperature of 37 °C, and they all controlled the indentation depth (I-mode). In I-mode, the constraint set by a user is a specific indentation depth value to be reached during the loading phase, while the displacements of the probe and of the cantilever bending are recorded. The I-mode allows users to perform stress–relaxation tests, which were essential for evaluating the time-dependent behaviors of the samples. Stress–relaxation tests consist of measuring the load relaxation over time in response to a constant value of indentation depth, which has to be reached rapidly. The change in load, required to maintain the imposed strain field, is measured during the holding phase. The experimental data we obtained were then used to evaluate the viscoelastic properties of the tested samples.

In our case, the value of δ was set to between 1 μm and 5 μm, and the indentation rate values (ρ) were selected to reach this value as fast as possible, i.e., ρ = 10–20 μm/s. The holding time was set to be equal to 5 s for all the experiments. For each sample, 50 indentations were performed, and 11 indentation curves were selected for the analysis.

2.3. Theoretical Remarks

For obtaining the mechanical properties of the samples from the analysis of their nanoindentation data, models arising from the contact mechanics theory were adopted. The Hertz model and the Oliver and Pharr model are the most commonly used models [57]. The latter is suitable for analyzing the responses of hard materials, while the Hertz model can be applied to predict the behaviors of soft materials during the first part of the loading phase, which is related to the elastic region. Considering the spherical tip of the probe

and the flat surface of the sample, the Hertz model stated the relation between P and δ as follows:

$$P = \frac{4}{3} \cdot E_{eff} \cdot R^{\frac{1}{2}} \cdot \delta^{\frac{3}{2}}, \tag{3}$$

where E_{eff} is the effective modulus of the contacting bodies (probe and sample), which is defined as follows:

$$\frac{1}{E_{eff}} = \frac{\left(1 - \nu_{sample}^2\right)}{E_{sample}} + \frac{\left(1 - \nu_{probe}^2\right)}{E_{probe}}, \tag{4}$$

where ν_{sample} and ν_{probe} are the Poisson coefficients of the sample and the probe, respectively, and E_{sample} and E_{probe} are the Young's moduli of the sample and the probe, respectively. Typically, a probe is made of a much harder material than a sample ($E_{probe} \gg E_{sample}$), and thus, Equation (4) can be rewritten as follows:

$$\frac{1}{E_{eff}} = \frac{\left(1 - \nu_{sample}^2\right)}{E_{sample}}. \tag{5}$$

As regards the viscoelastic responses of materials, different constitutive models have been developed to predict them. In this study, the generalized Maxwell model, which is mathematically described by the Prony series, was selected [54–56]. The analytical formulation describing the load decay during the holding phase as a function of time is reported below:

$$P(t) = P_\infty + \sum_{k=1}^{N} P_k \cdot e^{-\frac{t}{\tau_k}} \qquad N = 2, \tag{6a}$$

where $P_{(t = \infty)} = P_\infty$ is the equilibrium load, which is the value at the end of the relaxation time, and in this case, it was set as $t = 5$ s. The P_k parameters are the material parameters, while the τ_k parameters are the time parameters, and these represent the 4 parameters of the Prony series to be optimized through the fitting procedure.

Alternatively, Equation (6a) can be rewritten as follows:

$$P(t) = P_0 \cdot \left(1 - \sum_{k=1}^{N} P_k \cdot \left(1 - e^{-\frac{t}{\tau_k}}\right)\right) \qquad N = 2, \tag{6b}$$

where $P(t = 0) \equiv P_0 = P_{max}$ is the maximum load, which is the value at the beginning of the holding period (Figure 2b).

Using only one Maxwell element ($N = 1$), the fitting was unsatisfactory (see Appendix A); therefore, a second order Prony series was selected. This behavior was likely related to the principal constituents of the tested biological tissues, i.e., the highly cross-linked collagen and the elastic fibers [58], which were responsible for the different relaxation times.

Considering the relationship between the Young's modulus and the shear modulus G and the conventional assumption of the incompressibility of the tested samples ($\nu = 0.5$), we determined the following:

$$E_{sample} = 2G \cdot \left(1 + \nu_{sample}\right) \;\rightarrow\; E_{sample} = 3G. \tag{7}$$

Consequently, the link between the effective Young's modulus of the sample (E_{eff}) and the shear modulus of the sample was resolved using $E_{eff} = 4G$. Equation (3) could then become:

$$P = \frac{16}{9} \cdot G \cdot R^{\frac{1}{2}} \cdot \delta^{\frac{3}{2}}. \tag{8}$$

Finally, the G_k parameters that described the variation in the mechanical properties of the samples, i.e., the constitutive model, were calculated by combining the parameters P_1 and P_2 of the Prony series and inverting Equation (8), as follows:

$$G_k = \frac{P_k}{\frac{16}{3} \cdot R^{\frac{1}{2}} \cdot \delta_{max}^{\frac{3}{2}} \cdot \beta_k} \quad , \tag{9}$$

where β_k is the correction factor adopted to compensate for the finite ramp time, which can be expressed as follows [55,56]:

$$\beta_k = \begin{cases} \frac{\tau_k}{t_R} \cdot \left(e^{-\frac{t_R}{\tau_k}} - 1 \right) & k > 0, \\ \\ 1 & k = 0 \end{cases} \quad . \tag{10}$$

Finally, the constitutive model, i.e., the relaxation modulus, was derived as function of time, as follows:

$$G(t) = G_0 \cdot \left(1 - \sum_{k=1}^{N} G_k \cdot \left(1 - e^{-\frac{t}{\tau_k}} \right) \right) \quad N = 2 \,, \tag{11}$$

where $G(t = 0) \equiv G_0$ represents the instantaneous shear modulus corresponding to the maximum load at the beginning of the relaxation time. Using G_1 and G_2, deduced from Equation (9), in Equation (11), it was possible to calculate the value of the equilibrium shear modulus ($G(t = \infty) \equiv G_\infty$). The extent of the difference between the instantaneous (G_0) and equilibrium (G_∞) shear moduli values was an indication of the viscoelastic properties of the analyzed samples. Additionally, the viscosity parameters can be easily derived from the relaxation time:

$$\tau_k = \frac{\eta_k}{G_k} \quad \rightarrow \quad \eta_k = G_k \cdot \tau_k. \tag{12}$$

2.4. Fitting Procedure

The genetic algorithm (GA) approach was selected as the optimization tool to fit the experimental data through the built-in function in the Matlab® software R2023a. It is worth noting that Equation (6b), used to build the objective function, was normalized with respect to the maxim load value (P_{max}), as follows:

$$\frac{P(t)}{P_0} = 1 - p_1 \cdot \left(1 - e^{-\frac{t}{\tau_1}} \right) - p_2 \cdot \left(1 - e^{-\frac{t}{\tau_2}} \right) \,, \tag{13}$$

where $p_1 = P_1/P_0$ and $p_2 = P_2/P_0$. The following four parameters were: the two material parameters (p_1 and p_2) and the two time parameters (τ_1 and τ_2). The optimization process, schematized in Figure 4, began by filling the initial population needed by the GA with randomly generated sets of parameters, followed by determining some heuristic solutions. Random initialization has been proven to reduce the risk of obtaining very similar solutions that occur in local minima [50–52]. Furthermore, a lower and an upper boundary were set for the design variables through a series or preliminary simulations in order to confine the searching space to values with a physical meaning, thereby optimizing the computational cost.
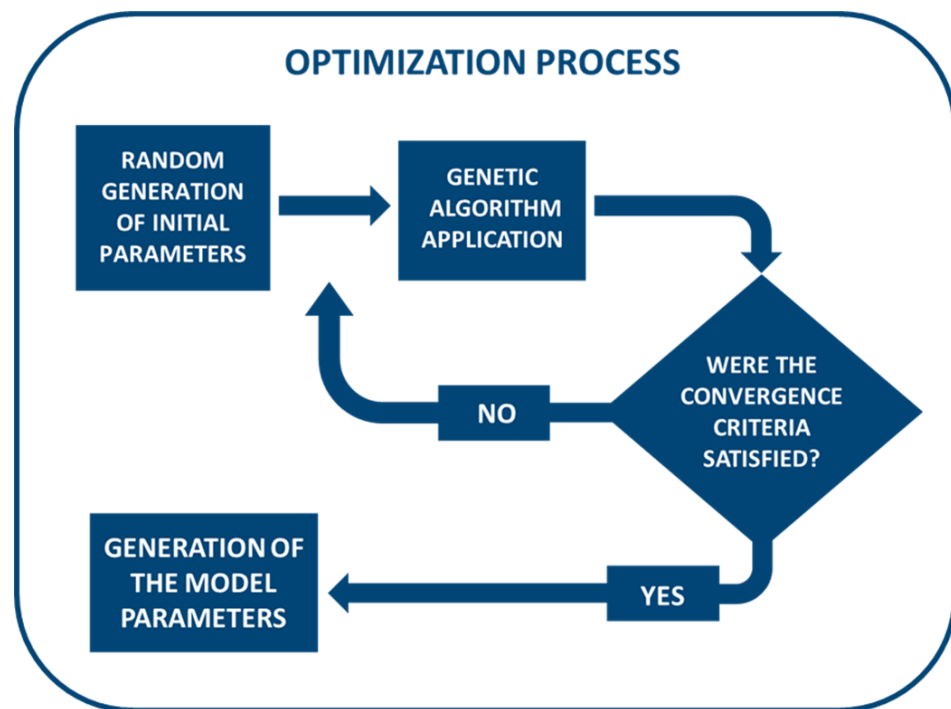
Figure 4. Schematization of the optimization process for fitting the experimental data.

The experimental data obtained through the nanoindentation tests were provided as inputs to the GA. A set of 11 experimental curves was considered for each sample. The algorithm was implemented in order to obtain 15 solutions for each curve. This allowed us to evaluate the dispersion of the computed solutions and the efficacy of the adopted method. Finally, the mean value of the 15 solutions was determined in order to provide a representative solution for each of the 11 analyzed curves. Then, one final set of four parameters (global parameters) was obtained as an average value of the eleven sets of solutions achieved for each sample.

2.5. Statistics

The efficacy of the proposed model in fitting the experimental data was evaluated through the coefficient of determination (R^2), commonly defined as follows:

$$R^2 = 1 - \frac{SS_{res}}{SS_{tot}},$$ (14)

where SS_{res} is the sum of the squares of the residuals, which is proportional to the variance of the residuals, while SS_{tot} is the total sum of the squares proportional to the variance in the data. The solution where $R^2 > 95\%$ was the only one accepted.

The normal distribution of the solutions, which resulted from the optimization process, was assessed by applying the Kolmogorov–Smirnov method. The distribution of the 15 values of each parameter for each curve, computed with a significance level of 5% ($p = 0.05$), was found to be normal. Then, due to the non-normality of the distribution of the parameters when grouped, the non-parametric Kruskal–Wallis test was adopted to compare the results, and the differences were considered significant when $p < 0.01$. The statistical analysis was performed using Matlab® software R2023a.

3. Results

3.1. Fitting Procedure

The explanatory stress–relaxation nanoindentation data and the fitting curves predicted by the Prony series are reported in Figure 5, showing the very good agreement between the experimental and the modelled data.
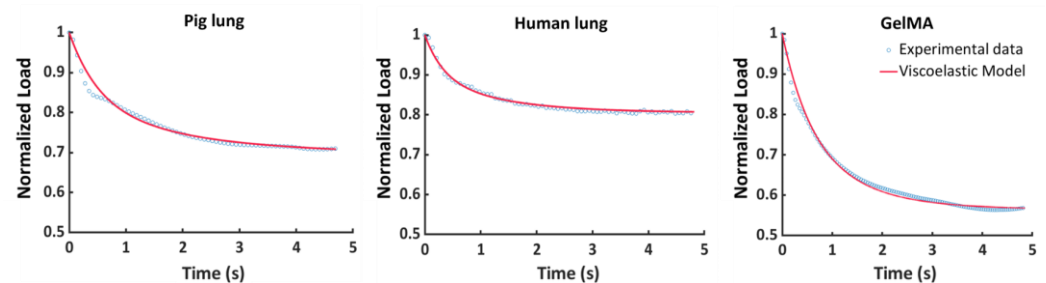
Figure 5. Representative experimental and superimposed fitted curves for the tested samples, showing the goodness of the fitting method.

3.2. Stress–Relaxation Behavior

Figure 6 shows the experimental stress–relaxation nanoindentation data gathered during the holding phase of the test for the tested materials. The average response of the tested samples is reported as a red line, and it was obtained using the global parameters (i.e., the mean values of the material and time parameters listed in Table 1) as input values for Equation (6b). Interestingly, for all the tested samples, two relaxation phases could be observed, i.e., an early non-linear decrease in the load, followed by linear decay until equilibrium was reached. This could be ascribed to the stress decrease related to the deformation and motion of the material polymer chains [59].
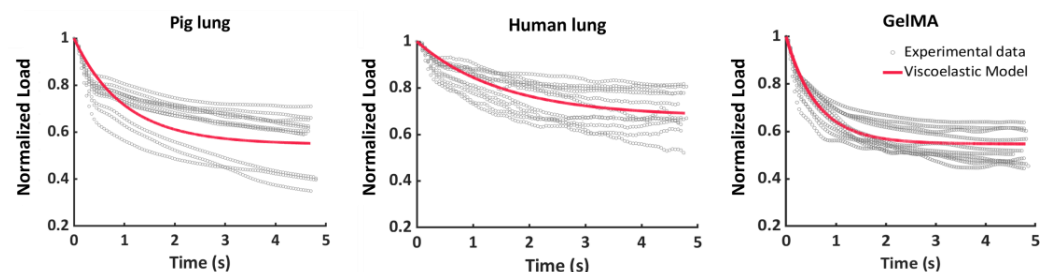

Figure 6. Representation of the samples' experimental curves overlapped with the fitted curves obtained with the global parameters of each sample.

Table 1. Global parameters: the average values with the standard deviations of the material (p) and time (τ) parameters for all the tested samples.

Parameters	Pig Lung	Human Lung	GelMA
p_1	0.22 ± 0.09	0.16 ± 0.09	0.22 ± 0.09
p_2	0.23 ± 0.12	0.16 ± 0.11	0.25 ± 0.10
τ_1 (s)	1.22 ± 0.77	1.37 ± 0.78	1.04 ± 0.42
τ_2 (s)	0.84 ± 0.76	1.76 ± 0.90	1.07 ± 0.42

The comparison of the average relaxation responses of the tested samples is shown in Figure 7. The behaviors of the pig lung and GelMA samples were characterized by similar decreases in the load, while for the human lung samples, the load decay appeared to be lesser than the other two samples.
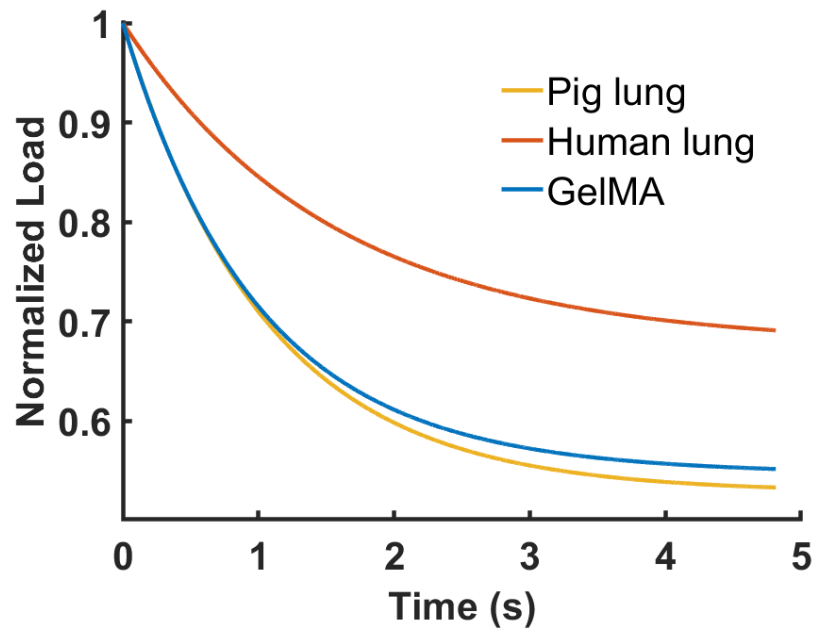
Figure 7. Comparison of the samples' behaviors modelled with the average values of the material and time parameters.

Figure 8 shows the contribution of the relaxation time (τ) of the Prony series for the low and high values found in this study, as reported in Figure 9. The higher the values for τ, the longer the periods necessary for relaxing the stresses.
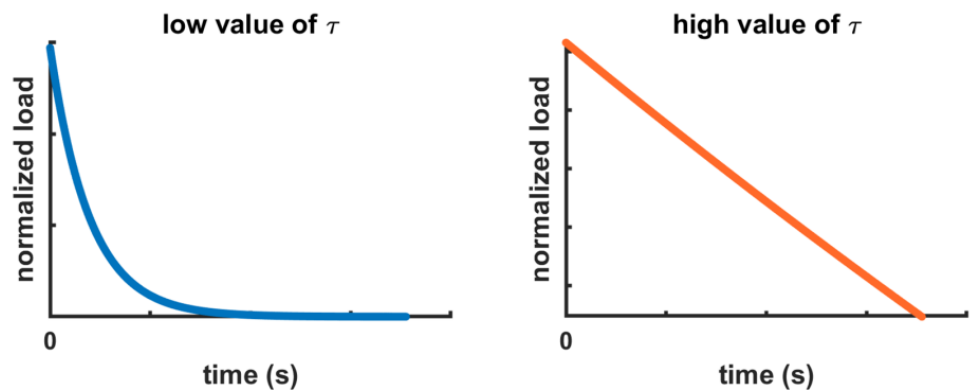
Figure 8. Explanatory curves of the exponential behaviors with the low and high values for τ found in this study.

Violin plots were selected to represent the distributions of the material and time parameters obtained through the fitting procedure, including all 15 of the solution sets for each of the analyzed experimental curves (Figure 9). The distributions of the material parameters p_1 and p_2 were normal for all the tested samples (Figure 9a). Differently, for the time parameters, evident bimodal distributions could be appreciated for the pig lung and human lung samples, whereas for the GelMA samples, although a bimodal distribution was present, it was considerably less pronounced (Figure 9b).
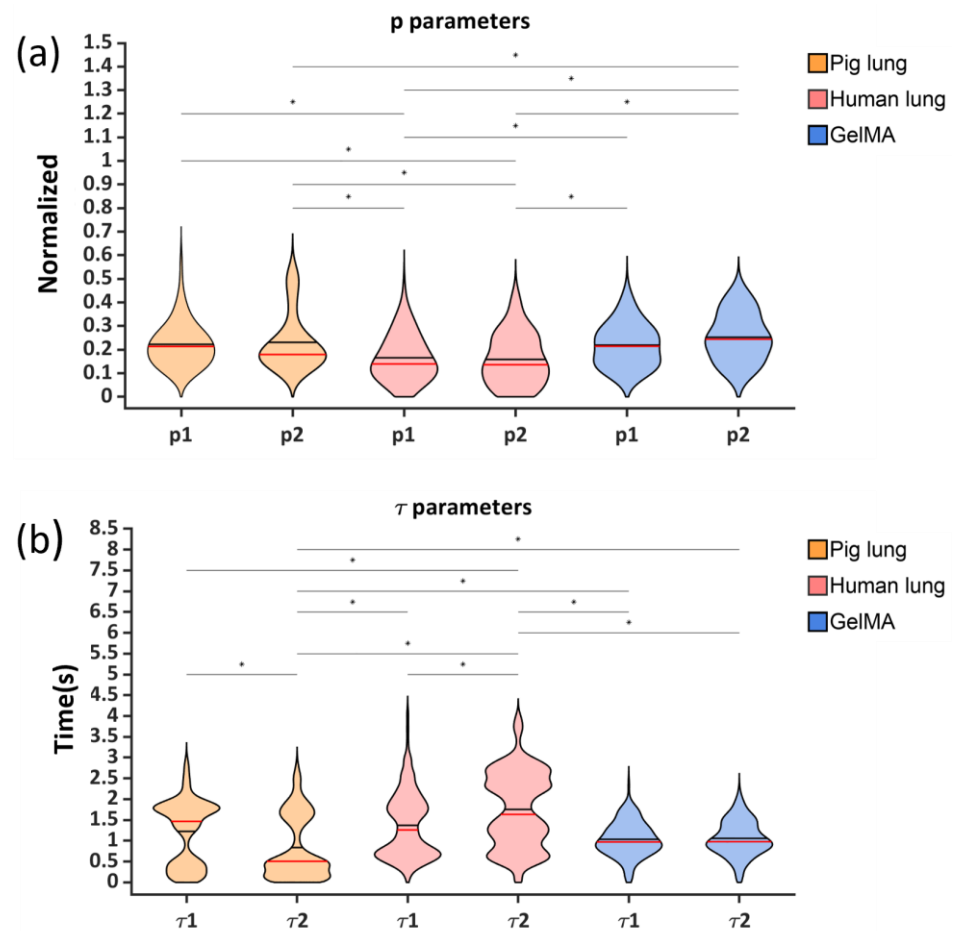
Figure 9. Violin plots of the p_1 and p_2 material parameters (**a**) and of the τ_1 and τ_2 time parameters (**b**) for all the obtained sets of possible solutions. The red and black lines indicate the median and the mean values, respectively.

The bimodal distributions of the relaxation times are a direct consequence of the dispersion of the experimental data shown in Figure 6. It is worth noting that the two peaks characterizing the distribution of the time parameters were not the result of the implemented optimization algorithm since the normality of the parameters obtained for each curve had been verified. Furthermore, the statistical analysis, as reported in Figure 9, highlighted that there were no statistical differences ($p > 0.01$) between the material parameters of the samples (no intravariability), but there was significant intervariability ($p < 0.01$). On the other hand, the time parameters showed intravariability only for the biological samples ($p < 0.01$), with no statistical differences were found between the time parameters characterizing the GelMA samples. Moreover, only the time parameter results for τ_2 were statistically different among all the samples.

A quantitative comparison of the samples' behaviors was carried out by considering the instantaneous and equilibrium shear moduli (G_0 and G_∞, Figure 10a) and the viscosity parameters (η_1 and η_2, Figure 10b). The GelMA samples showed the highest values for G_0 and the most pronounced reduction in the relaxation modulus (the difference between G_0 and G_∞), while for the pig and human lung samples, the decrease was less evident. The highest values obtained for the viscosity parameters could have indicated that the GelMA samples were characterized by a more solid-like behavior than the biological samples. The mean values and standard deviations of the relaxation moduli and of the viscosity parameters of each tested sample are reported in Table 2 and Table 3, respectively.
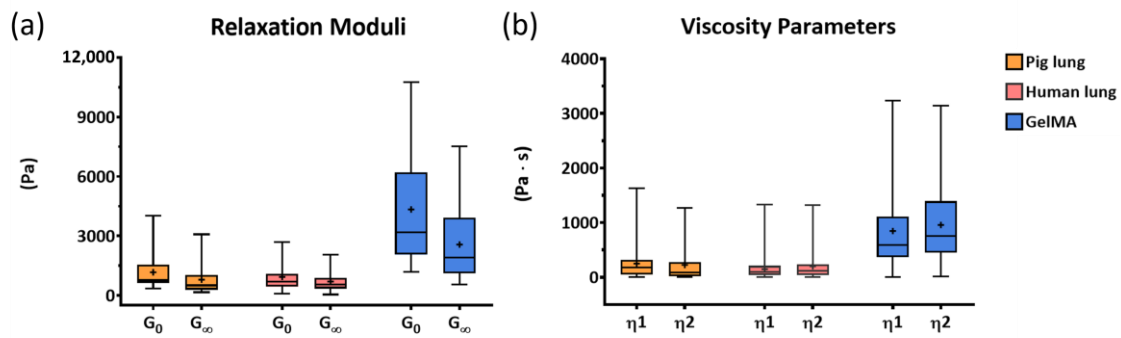
Figure 10. Boxplots of the mechanical properties describing the constitutive model of the analyzed samples: relaxation moduli (**a**) and viscosity (**b**) parameters.

Table 2. Mean values and standard deviations of the instantaneous and equilibrium relaxation moduli.

Sample	G_0 (Pa)	G_∞ (Pa)
Pig lung	1166.7 ± 995.5	792.7 ± 764.7
Human lung	929.1 ± 751.8	702.3 ± 548.2
GelMA	4339.2 ± 2689	2565 ± 1698

Table 3. Mean values and standard deviations of the viscosity parameters.

Sample	η_1 (Pa·s)	η_2 (Pa·s)
Pig lung	249.9 ± 263.4	225.7 ± 323.5
Human lung	148 ± 171.4	199.2 ± 262.6
GelMA	847.8 ± 733.1	957.2 ± 705.4

4. Discussion

Knowledge of the time-dependent mechanical behaviors of materials designed for mimicking native tissues is of paramount importance in the context of mechanobiology and tissue engineering research. Thus, in this study, we developed a methodological approach for extrapolating the characteristic mechanical parameters that describe the viscoelastic behaviors of soft biological tissues and hydrogels.

In particular, the proposed approach was based on the analysis of the stress–relaxation experimental curves that we obtained by adopting the nanoindentation technique and controlling the indentation depths to minimize variability in the results [60]. Samples of pig and human lung tissues and a specific GelMA hydrogel were tested, and their viscoelastic properties were quantified and compared. For each sample, several stress–relaxation curves were obtained and analyzed in order to evaluate the relaxation moduli (G_0 and G_∞) and the viscosity parameters in a straightforward and consistent way. Moreover, for the optimization of the experimental data-fitting, the genetic algorithm was demonstrated to be an effective and reliable choice. Indeed, the adopted approach allowed us to properly fit the experimental data (Figure 5) and identify the characteristic behaviors of the tested samples. The explanatory stress–relaxation curves (Figure 6) indicated that for all the samples, a holding period of 5 s was sufficient for reaching a complete relaxation of the stresses stored during the instantaneous loading phase at the cell-length scale. Studies conducted on biological samples at the macroscopic scale have shown that after an impulse load, a steady state could be reached in minutes or hours [61–63], though at the cell-length scale, the materials' responses change, as do the characteristic time-dependent responses.

From the comparison of the mean behaviors of the tested samples, faster decreases characterized the pig lung and GelMA samples compared to the human lung (Figure 7). The relaxation behavior, as reported in Equation (13), was determined by the following two

classes of parameters: (i) the material parameters, p_i, that took into account the amount of force reached at the prescribed deformation, and (ii) the time parameters, τ_{iI}, that controlled the relaxation rate (Figure 8). To identify and compare the potential differences in the relaxation mechanisms of the tested samples, the values of the time parameters were not assigned a priori with default values, as has been reported in the literature [11,64–66]. As regards the lung tissue, its mechanics were determined by the synergic interaction of all its constituents [63]. Accordingly, the adopted viscoelastic model highlighted the evident bimodal distribution of the time parameters of the biological samples (Figure 9), and the two peaks in the distribution could have represented the contribution of the most abundant molecular elements that characterized the microstructures of the biological samples, i.e., the ECM, which is made of highly cross-linked collagen and elastin [58], and the cells [59,67,68]. Generally, elastic fibers confer to tissues the capability to recover from deformation as soon as they are unloaded [63,69], and the highly cross-linked collagen and the cells would be responsible for the dissipation of the energy stored during the deformation [59,67,68], controlling, thus, the time-dependent behaviors of the biological samples. The intricate network formed by the elastic fibers, the highly cross-linked collagen [58], and the cells determined the viscoelastic responses of the biological samples here analyzed. As a matter of fact, the relaxation times τ_1 and τ_2 obtained for the biological samples resulted in significantly different values. However, further studies are required to understand the contribution of the elemental units that composed the tissues and which determined their time-dependent responses.

Comparing pig and human native lung tissues, Balestrini J. et al. [70] demonstrated consistent differences in the contents of their ECM components. In particular, when compared with pig lung tissue, human lung contains double amount of elastin fibers (30% vs. 15%) and half the amount of glicosaminoglycans (25% vs. 51%), while the percentage of collagen remains quite the same. Moreover, another study conducted by Burgstaller G. et al. [71], which widely analyzed the composition of lung ECM, highlighted the roles of elastin, collagen, and proteoglycans in providing elasticity, structural support and strength, and stability, respectively. The higher percentages of elastin in human lungs could explain the reduced tissue relaxation and, thus, the inferior load decay of the human lung compared to pig lung illustrated in Figure 7.

On the other hand, the GelMA samples showed a less-obvious bimodal distribution, and no statistical differences were found between the two time constants. The biggest peak of the violin plot related to the GelMA sample (Figure 9b) could be linked to the contribution of the most present molecular segment, i.e., bovine gelatin, while the contribution of the methacrylic anhydride did not appear to be impactful on the time-dependent response. As reported in the literature, in the context of hydrogels derived from proteins, their viscoelastic behaviors are strongly influenced by the unfolding of the molecular protein chains, which need to overcome friction from other chains [59,72,73]. This has led to the hypothesis that a higher concentration of bovine gelatin could control the time-dependent response of a hydrogel.

The absence of intravariability in the material parameters (p_1 and p_2) and, on the contrary, the intravariability in the time parameters reported in Figure 9 highlighted that the time-dependent characteristics were crucial in defining the mechanical behaviors at the cell-length scale. Furthermore, the GelMA hydrogel was produced in a formulation that conferred greater viscoelastic properties with respect to the analyzed biological samples, and it was characterized by one predominant relaxation mechanism. Despite this, the values of the time parameters found for the GelMA sample were in the same range as the biological samples. Further improvement will be implemented in the formulation of the GelMA hydrogel to obtain a more complex relaxing mechanism that better mimics the mechanical properties of lung tissue.

Despite the promising results obtained in this study, there is space for improvement. The implementation of a hyper-elastic model [55,56], even if this could introduce a higher number of parameters that are difficult to interpret, could better model the behaviors of

biological tissues and further improve our approach. However, the Hertz model adopted herein is one of the most common approaches in analogous studies and represents a satisfactory starting point that allowed us to obtain robust and reliable results. Moreover, in the future, the effect of the loading rate of the indentation test and how it could influence a material's response will be further investigated.

5. Conclusions

The proposed methodological approach allowed for the robust characterization and a comparison of the viscoelastic behaviors of soft biological tissues and a specific hydrogel at the micro scale, proving its versatility. Furthermore, for each sample, a constitutive model characterizing its time-dependent behavior was defined. In conclusion, through the proposed approach, a quantitative measure of the viscous properties of soft biological tissues and a hydrogel was obtained, evaluating the relaxation moduli and the viscous parameters. The potential of this approach is of considerable value for mechanotransduction studies as it can provide a powerful tool for defining the mechanical properties of the substrates developed to mimic ECM tissues.

Author Contributions: G.S. conceived the study; G.S., T.T. and D.M. conceived the experimental set-up; F.F., S.V. and D.B. manufactured the GelMA sample; V.M., B.P. and L.P. provided the biological expertise and the human sample; T.T. and G.S. performed the nanoindentation tests; M.T. and G.S. performed the data analysis; M.T. and G.S. reviewed the state of the art; M.T. prepared the figures; M.T., G.S. and D.M. wrote the manuscript; D.M., G.S. and A.A. reviewed the manuscript; F.P. and A.A. Resources. All authors have read and agreed to the published version of the manuscript.

Institutional Review Board Statement: The study was conducted in accordance with the Declaration of Helsinki and approved by the Institutional Review Board of the Candiolo Cancer Institute within the project PROFILING protocol no. 001-IRCC-00IIS-10.

Informed Consent Statement: Informed consent was obtained from all subjects involved in the study.

Data Availability Statement: Data are contained within the article. The raw data are available upon request to the corresponding author.

Conflicts of Interest: The authors declare no conflict of interest.

Appendix A

Figure A1 highlights the unsatisfactory results obtained by using a first-order Prony series as a fitting function for the GA optimization process. An R^2 lower than 95% was obtained for several curves, and therefore, the results were not acceptable. In particular, as shown in Figure A1, $R^2 = 74\%$ was obtained for the pig lung sample's representative curve, $R^2 = 89\%$ was reached for the human lung sample's representative curve, and $R^2 = 46\%$ was the result for the GelMA sample's explanatory curve.
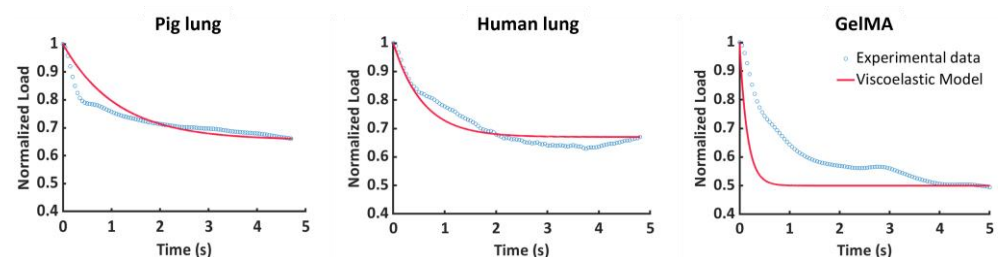
Figure A1. Representative experimental and superimposed fitted curves for the tested samples using the Prony series with one element ($N = 1$) as the fitting function.

References

1. Handorf, A.M.; Zhou, Y.; Halanski, M.A.; Li, W.J. Tissue Stiffness Dictates Development, Homeostasis, and Disease Progression. *Organogenesis* **2015**, *11*, 1–15. [CrossRef]
2. Di, X.; Gao, X.; Peng, L.; Ai, J.; Jin, X.; Qi, S.; Li, H.; Wang, K.; Luo, D. Cellular Mechanotransduction in Health and Diseases: From Molecular Mechanism to Therapeutic Targets. *Signal Transduct. Target. Ther.* **2023**, *8*, 282. [CrossRef]
3. Melica, M.E.; La Regina, G.L.; Parri, M.; Peired, A.J.; Romagnani, P.; Lasagni, L. Substrate Stiffness Modulates Renal Progenitor Cell Properties via a ROCK-Mediated Mechanotransduction Mechanism. *Cells* **2019**, *8*, 1561. [CrossRef]
4. Bakhshandeh, B.; Sorboni, S.G.; Ranjbar, N.; Deyhimfar, R.; Abtahi, M.S.; Izady, M.; Kazemi, N.; Noori, A.; Pennisi, C.P. Mechanotransduction in Tissue Engineering: Insights into the Interaction of Stem Cells with Biomechanical Cues. *Exp. Cell Res.* **2023**, *431*, 113766. [CrossRef]
5. Sridharan, R.; Cavanagh, B.; Cameron, A.R.; Kelly, D.J.; O'Brien, F.J. Material Stiffness Influences the Polarization State, Function and Migration Mode of Macrophages. *Acta Biomater.* **2019**, *89*, 47–59. [CrossRef]
6. Janmey, P.A.; Fletcher, D.A.; Reinhart-King, C.A. Stiffness Sensing by Cells. *Physiol. Rev.* **2020**, *100*, 695–724. [CrossRef]
7. Chin, L.K.; Xia, Y.; Discher, D.E.; Janmey, P.A. Mechanotransduction in Cancer. *Curr. Opin. Chem. Eng.* **2016**, *11*, 77–84. [CrossRef]
8. Montagner, G.; Barbazza, A.; Lugas, A.T.; Terzini, M.; Serino, G.; Bignardi, C.; Cacciatore, M.; Vida, V.L.; Padalino, M.A.; Trojan, D. Decellularized Cryopreserved Human Pericardium: A Validation Study towards Tissue Bank Practice. *Cell Tissue Bank.* **2023**. [CrossRef]
9. Belviso, I.; Romano, V.; Sacco, A.M.; Ricci, G.; Massai, D.; Cammarota, M.; Catizone, A.; Schiraldi, C.; Nurzynska, D.; Terzini, M.; et al. Decellularized Human Dermal Matrix as a Biological Scaffold for Cardiac Repair and Regeneration. *Front. Bioeng. Biotechnol.* **2020**, *8*, 229. [CrossRef]
10. Hamon, M.; Chen, Y.; Srivastava, P.; Chang, H.M.; Gupta, V.; Jin, L.; Yanagawa, N.; Hauser, P.V. Matrix Stiffness Influences Tubular Formation in Renal Tissue Engineering. *Appl. Sci.* **2023**, *13*, 4510. [CrossRef]
11. Islam, M.R.; Virag, J.; Oyen, M.L. Micromechanical Poroelastic and Viscoelastic Properties of Ex-Vivo Soft Tissues. *J. Biomech.* **2020**, *113*, 110090. [CrossRef] [PubMed]
12. Cacopardo, L.; Guazzelli, N.; Nossa, R.; Mattei, G.; Ahluwalia, A. Engineering Hydrogel Viscoelasticity. *J. Mech. Behav. Biomed. Mater.* **2019**, *89*, 162–167. [CrossRef] [PubMed]
13. Cantini, M.; Donnelly, H.; Dalby, M.J.; Salmeron-Sanchez, M. The Plot Thickens: The Emerging Role of Matrix Viscosity in Cell Mechanotransduction. *Adv. Healthc. Mater.* **2020**, *9*, 1901259. [CrossRef] [PubMed]
14. Chaudhuri, O.; Cooper-White, J.; Janmey, P.A.; Mooney, D.J.; Shenoy, V.B. Effects of Extracellular Matrix Viscoelasticity on Cellular Behaviour. *Nature* **2020**, *584*, 535–546. [CrossRef] [PubMed]
15. Zhang, Y.; Wang, Z.; Sun, Q.; Li, Q.; Li, S.; Li, X. Dynamic Hydrogels with Viscoelasticity and Tunable Stiffness for the Regulation of Cell Behavior and Fate. *Materials* **2023**, *16*, 5161. [CrossRef] [PubMed]
16. Li, J.; Liu, Y.; Zhang, Y.; Yao, B.; Enhejirigala, B.; Li, Z.; Song, W.; Wang, Y.; Duan, X.; Yuan, X.; et al. Biophysical and Biochemical Cues of Biomaterials Guide Mesenchymal Stem Cell Behaviors. *Front. Cell Dev. Biol.* **2021**, *9*, 640388. [CrossRef]
17. Goetzke, R.; Sechi, A.; De Laporte, L.; Neuss, S.; Wagner, W. Why the Impact of Mechanical Stimuli on Stem Cells Remains a Challenge. *Cell. Mol. Life Sci.* **2018**, *75*, 3297–3312. [CrossRef]
18. Puech, P.H.; Bongrand, P. Mechanotransduction as a Major Driver of Cell Behaviour: Mechanisms, and Relevance to Cell Organization and Future Research. *Open Biol.* **2021**, *11*, 210256. [CrossRef]
19. Díaz-Bello, B.; Monroy-Romero, A.X.; Pérez-Calixto, D.; Zamarrón-Hernández, D.; Serna-Marquez, N.; Vázquez-Victorio, G.; Hautefeuille, M. Method for the Direct Fabrication of Polyacrylamide Hydrogels with Controlled Stiffness in Polystyrene Multiwell Plates for Mechanobiology Assays. *ACS Biomater. Sci. Eng.* **2019**, *5*, 4219–4227. [CrossRef]
20. Tse, J.R.; Engler, A.J. Preparation of Hydrogel Substrates with Tunable Mechanical Properties. *Curr. Protoc. Cell Biol.* **2010**, *47*, 10–16. [CrossRef]
21. Ho, T.C.; Chang, C.C.; Chan, H.P.; Chung, T.W.; Shu, C.W.; Chuang, K.P.; Duh, T.H.; Yang, M.H.; Tyan, Y.C. Hydrogels: Properties and Applications in Biomedicine. *Molecules* **2022**, *27*, 2902. [CrossRef]
22. Kocen, R.; Gasik, M.; Gantar, A.; Novak, S. Viscoelastic Behaviour of Hydrogel-Based Composites for Tissue Engineering under Mechanical Load. *Biomed. Mater.* **2017**, *12*, 025004. [CrossRef]
23. Mierke, C.T. Viscoelasticity, Like Forces, Plays a Role in Mechanotransduction. *Front. Cell Dev. Biol.* **2022**, *10*, 789841. [CrossRef]
24. Cacopardo, L.; Guazzelli, N.; Ahluwalia, A. Characterizing and Engineering Biomimetic Materials for Viscoelastic Mechanotransduction Studies. *Tissue Eng. Part B Rev.* **2022**, *28*, 912–925. [CrossRef] [PubMed]
25. Barthes, J.; Özçelik, H.; Hindié, M.; Ndreu-Halili, A.; Hasan, A.; Vrana, N.E. Cell Microenvironment Engineering and Monitoring for Tissue Engineering and Regenerative Medicine: The Recent Advances. *BioMed Res. Int.* **2014**, *2014*, 921905. [CrossRef]
26. Bilston, L.E. Soft Tissue Rheology and Its Implications for Elastography: Challenges and Opportunities. *NMR Biomed.* **2018**, *31*, e3832. [CrossRef]
27. Urban, M.W. Production of Acoustic Radiation Force Using Ultrasound: Methods and Applications. *Expert. Rev. Med. Devices* **2018**, *15*, 819–834. [CrossRef]
28. Li, G.Y.; Cao, Y. Mechanics of Ultrasound Elastography. *Proc. R. Soc. A Math. Phys. Eng. Sci.* **2017**, *473*, 20160841. [CrossRef] [PubMed]

29. Itoh, A.; Ueno, E.; Tohno, E.; Kamma, H.; Takahashi, H.; Shiina, T.; Yamakawa, M.; Matsumura, T. Breast Disease: Clinical Application of US Elastography for Diagnosis. *Radiology* **2006**, *239*, 341–350. [CrossRef]

30. Jugé, L.; Foley, P.; Hatt, A.; Yeung, J.; Bilston, L.E. Ex Vivo Bovine Liver Nonlinear Viscoelastic Properties: MR Elastography and Rheological Measurements. *J. Mech. Behav. Biomed. Mater.* **2023**, *138*, 105638. [CrossRef] [PubMed]

31. McKnight, A.L.; Kugel, J.L.; Rossman, P.J.; Manduca, A.; Hartmann, L.C.; Ehman, R.L. MR Elastography of Breast Cancer: Preliminary Results. *Am. J. Roentgenol.* **2012**, *178*, 1411–1417. [CrossRef]

32. Larin, K.V.; Sampson, D.D. Optical Coherence Elastography–OCT at Work in Tissue Biomechanics [Invited]. *Biomed. Opt. Express* **2017**, *8*, 1172. [CrossRef] [PubMed]

33. Han, Z.; Singh, M.; Aglyamov, S.R.; Liu, C.-H.; Nair, A.; Raghunathan, R.; Wu, C.; Li, J.; Larin, K.V. Quantifying Tissue Viscoelasticity Using Optical Coherence Elastography and the Rayleigh Wave Model. *J. Biomed. Opt.* **2016**, *21*, 090504. [CrossRef]

34. Leartprapun, N.; Iyer, R.; Adie, S.G. Model-Independent Quantification of Soft Tissue Viscoelasticity with Dynamic Optical Coherence Elastography. *Proc. SPIE* **2017**, *10053*, 1005322.

35. Raghunathan, S.; Evans, D.; Sparks, J.L. Poroviscoelastic Modeling of Liver Biomechanical Response in Unconfined Compression. *Ann. Biomed. Eng.* **2010**, *38*, 1789–1800. [CrossRef]

36. Miller, K. Method of Testing Very Soft Biological Tissues in Compression. *J. Biomech.* **2005**, *38*, 153–158. [CrossRef]

37. López-Guerra, E.A.; Solares, S.D. Modeling Viscoelasticity through Spring-Dashpot Models in Intermittent-Contact Atomic Force Microscopy. *Beilstein J. Nanotechnol.* **2014**, *5*, 2149–2163. [CrossRef]

38. Najera, J.; Rosenberger, M.R.; Datta, M. Atomic Force Microscopy Methods to Measure Tumor Mechanical Properties. *Cancers* **2023**, *15*, 3285. [CrossRef]

39. Abuhattum, S.; Mokbel, D.; Müller, P.; Soteriou, D.; Guck, J.; Aland, S. An Explicit Model to Extract Viscoelastic Properties of Cells from AFM Force-Indentation Curves. *iScience* **2022**, *25*, 104016. [CrossRef]

40. Efremov, Y.M.; Okajima, T.; Raman, A. Measuring Viscoelasticity of Soft Biological Samples Using Atomic Force Microscopy. *Soft Matter* **2019**, *16*, 64–81. [CrossRef]

41. Qian, L.; Zhao, H. Nanoindentation of Soft Biological Materials. *Micromachines* **2018**, *9*, 654. [CrossRef]

42. Oyen, M.L.; Shean, T.A.V.; Strange, D.G.T.; Galli, M. Size Effects in Indentation of Hydrated Biological Tissues. *J. Mater. Res.* **2012**, *27*, 245–255. [CrossRef]

43. Mijailovic, A.S.; Qing, B.; Fortunato, D.; Van Vliet, K.J. Characterizing Viscoelastic Mechanical Properties of Highly Compliant Polymers and Biological Tissues Using Impact Indentation. *Acta Biomater.* **2018**, *71*, 388–397. [CrossRef]

44. Kazaili, A.; Geraghty, B.; Akhtar, R. Microscale Assessment of Corneal Viscoelastic Properties under Physiological Pressures. *J. Mech. Behav. Biomed. Mater.* **2019**, *100*, 103375. [CrossRef] [PubMed]

45. Huang, H.; Tang, W.; Yang, Y.; Wu, B.; Yan, B. Determination of Viscoelastic Properties of the Periodontal Ligament Using Nanoindentation Testing and Numerical Modeling. *J. Mech. Med. Biol.* **2016**, *16*, 1650089. [CrossRef]

46. Park, K.; Lonsberry, G.E.; Gearing, M.; Levey, A.I.; Desai, J.P. Viscoelastic Properties of Human Autopsy Brain Tissues as Biomarkers for Alzheimer's Diseases. *IEEE Trans. Biomed. Eng.* **2019**, *66*, 1705–1713. [CrossRef] [PubMed]

47. Mattei, G.; Gruca, G.; Rijnveld, N.; Ahluwalia, A. The Nano-Epsilon Dot Method for Strain Rate Viscoelastic Characterisation of Soft Biomaterials by Spherical Nano-Indentation. *J. Mech. Behav. Biomed. Mater.* **2015**, *50*, 150–159. [CrossRef]

48. Jiri, N.; Michael, S.; Philipp, E. Micromechanical Properties of Polyacrylamide Hydrogels Measured by Spherical Nanoindentation. *Key Eng. Mater.* **2014**, *606*, 121–124.

49. Simič, R.; Mathis, C.H.; Spencer, N.D. A Two-Step Method for Rate-Dependent Nano-Indentation of Hydrogels. *Polymer* **2018**, *137*, 276–282. [CrossRef]

50. Karr, C.L.; Weck, B.; Massart, D.L.; Vankeerberghen, P. Least Median Squares Curve Fitting Using a Genetic Algorithm. *Eng. Appl. Artif. Intell.* **1995**, *8*, 177–189. [CrossRef]

51. Agapie, A.; Fagarasan, F.; Stanciulescu, B. A Genetic Algorithm for a Fitting Problem. *Nucl. Instrum. Methods Phys. Res. A* **1997**, *389*, 288–292. [CrossRef]

52. Smith, A.E.; Gulsen, M.; Tate, D.M. A Genetic Algorithm Approach to Curve Fitting. *Int. J. Prod. Res.* **1995**, *33*, 1911–1923.

53. Van Den Bulcke, A.I.; Bogdanov, B.; De Rooze, N.; Schacht, E.H.; Cornelissen, M.; Berghmans, H. Structural and Rheological Properties of Methacrylamide Modified Gelatin Hydrogels. *Biomacromolecules* **2000**, *1*, 31–38. [CrossRef] [PubMed]

54. Mattice, J.M.; Lau, A.G.; Oyen, M.L.; Kent, R.W. Spherical Indentation Load-Relaxation of Soft Biological Tissues. *J. Mater. Res.* **2006**, *21*, 2003–2010. [CrossRef]

55. Qiang, B.; Greenleaf, J.; Oyen, M.; Zhang, X. Estimating Material Elasticity by Spherical Indentation Load-Relaxation Tests on Viscoelastic Samples of Finite Thickness. *IEEE Trans. Ultrason. Ferroelectr. Freq. Control* **2011**, *58*, 1418–1429. [CrossRef]

56. Strange, D.G.T.; Fletcher, T.L.; Tonsomboon, K.; Brawn, H.; Zhao, X.; Oyen, M.L. Separating Poroviscoelastic Deformation Mechanisms in Hydrogels. *Appl. Phys. Lett.* **2013**, *102*, 031913. [CrossRef]

57. Hertz, H. On the Contact of Elastic Solids. *J. Für Die Reine Und Angew. Math.* **1881**, *92*, 156–171.

58. Muiznieks, L.D.; Keeley, F.W. Molecular Assembly and Mechanical Properties of the Extracellular Matrix: A Fibrous Protein Perspective. *Biochim. Biophys. Acta Mol. Basis Dis.* **2013**, *1832*, 866–875. [CrossRef] [PubMed]

59. Huang, D.; Huang, Y.; Xiao, Y.; Yang, X.; Lin, H.; Feng, G.; Zhu, X.; Zhang, X. Viscoelasticity in Natural Tissues and Engineered Scaffolds for Tissue Reconstruction. *Acta Biomater.* **2019**, *97*, 74–92. [CrossRef]

60. Alisafaei, F.; Han, C.S.; Sanei, S.H.R. On the Time and Indentation Depth Dependence of Hardness, Dissipation and Stiffness in Polydimethylsiloxane. *Polym. Test.* **2013**, *32*, 1220–1228. [CrossRef]

61. Forgacs, G.; Foty, R.A.; Shafrir, Y.; Steinberg, M.S. Viscoelastic Properties of Living Embryonic Tissues: A Quantitative Study. *Biophys. J.* **1998**, *74*, 2227–2234. [CrossRef]

62. Dwivedi, K.K.; Lakhani, P.; Kumar, S.; Kumar, N. The Effect of Strain Rate on the Stress Relaxation of the Pig Dermis: A Hyper-Viscoelastic Approach. *J. Biomech. Eng.* **2020**, *142*, 091006. [CrossRef]

63. Suki, B.; Bates, J.H.T. Emergent Behavior in Lung Structure and Function Lung Tissue Mechanics as an Emergent Phenomenon. *J. Appl. Physiol.* **2011**, *110*, 1111–1118. [CrossRef]

64. Kauer, M.; Vuskovic, V.; Dual, J.; Szekely, G.; Bajka, M. Inverse Finite Element Characterization of Soft Tissues. *Med. Image Anal.* **2002**, *6*, 275–287. [CrossRef]

65. Lucas, S.R.; Bass, C.R.; Salzar, R.S.; Oyen, M.L.; Planchak, C.; Ziemba, A.; Shender, B.S.; Paskoff, G. Viscoelastic Properties of the Cervical Spinal Ligaments under Fast Strain-Rate Deformations. *Acta Biomater.* **2008**, *4*, 117–125. [CrossRef] [PubMed]

66. Troyer, K.L.; Estep, D.J.; Puttlitz, C.M. Viscoelastic Effects during Loading Play an Integral Role in Soft Tissue Mechanics. *Acta Biomater.* **2012**, *8*, 234–243. [CrossRef]

67. Rigato, A.; Miyagi, A.; Scheuring, S.; Rico, F. High-Frequency Microrheology Reveals Cytoskeleton Dynamics in Living Cells. *Nat. Phys.* **2017**, *13*, 771–775. [CrossRef]

68. Hampoelz, B.; Lecuit, T. Nuclear Mechanics in Differentiation and Development. *Curr. Opin. Cell Biol.* **2011**, *23*, 668–675. [CrossRef] [PubMed]

69. Gosline, J.; Lillie, M.; Carrington, E.; Guerette, P.; Ortlepp, C.; Savage, K. Elastic Proteins: Biological Roles and Mechanical Properties. *Philos. Trans. R. Soc. B Biol. Sci.* **2002**, *357*, 121–132. [CrossRef] [PubMed]

70. Balestrini, J.L.; Gard, A.L.; Gerhold, K.A.; Wilcox, E.C.; Liu, A.; Schwan, J.; Le, A.V.; Baevova, P.; Dimitrievska, S.; Zhao, L.; et al. Comparative Biology of Decellularized Lung Matrix: Implications of Species Mismatch in Regenerative Medicine. *Biomaterials* **2016**, *102*, 220–230. [CrossRef]

71. Burgstaller, G.; Oehrle, B.; Gerckens, M.; White, E.S.; Schiller, H.B.; Eickelberg, O. The Instructive Extracellular Matrix of the Lung: Basic Composition and Alterations in Chronic Lung Disease. *Eur. Respir. J.* **2017**, *50*, 1601805. [CrossRef] [PubMed]

72. Brown, A.E.X.; Litvinov, R.I.; Discher, D.E.; Purohit, P.K.; Weisel, J.W. Multiscale Mechanics of Fibrin Polymer: Gel Stretching with Protein Unfolding and Loss of Water. *Science* **2009**, *325*, 741–744. [CrossRef] [PubMed]

73. Chaudhuri, O.; Gu, L.; Darnell, M.; Klumpers, D.; Bencherif, S.A.; Weaver, J.C.; Huebsch, N.; Mooney, D.J. Substrate Stress Relaxation Regulates Cell Spreading. *Nat. Commun.* **2015**, *6*, 6365. [CrossRef] [PubMed]